

Accepted Manuscript

Alternating current (AC) susceptibility as a particle-focused probe of coating and clustering behaviour in magnetic nanoparticle suspensions

Kaarjel K. Narayanasamy, Melissa Cruz-Acuña, Carlos Rinaldi, James Everett, Jon Dobson, Neil D. Telling

PII: S0021-9797(18)30920-2
DOI: <https://doi.org/10.1016/j.jcis.2018.08.014>
Reference: YJCIS 23947

To appear in: *Journal of Colloid and Interface Science*

Received Date: 15 May 2018
Revised Date: 6 August 2018
Accepted Date: 6 August 2018

Please cite this article as: K.K. Narayanasamy, M. Cruz-Acuña, C. Rinaldi, J. Everett, J. Dobson, N.D. Telling, Alternating current (AC) susceptibility as a particle-focused probe of coating and clustering behaviour in magnetic nanoparticle suspensions, *Journal of Colloid and Interface Science* (2018), doi: <https://doi.org/10.1016/j.jcis.2018.08.014>

This is a PDF file of an unedited manuscript that has been accepted for publication. As a service to our customers we are providing this early version of the manuscript. The manuscript will undergo copyediting, typesetting, and review of the resulting proof before it is published in its final form. Please note that during the production process errors may be discovered which could affect the content, and all legal disclaimers that apply to the journal pertain.



Alternating current (AC) susceptibility as a particle-focused probe of coating and clustering behaviour in magnetic nanoparticle suspensions

Kaarjel K. Narayanasamy^{1,2,*} (k.k.narayanasamy@leeds.ac.uk)

Melissa Cruz-Acuña² (mcruz@ufl.edu)

Carlos Rinaldi² (carlos.rinaldi@bme.ufl.edu)

James Everett¹ (j.everett@keele.ac.uk)

Jon Dobson^{2,3} (jdobson@bme.ufl.edu)

Neil D. Telling¹ (n.d.telling@keele.ac.uk)

¹ Institute for Science and Technology in Medicine, Keele University, Stoke-on-Trent, Staffordshire ST4 7QB, United Kingdom.

² J. Crayton Pruitt Family Department of Biomedical Engineering, University of Florida, Gainesville, Florida 32611, United States.

³ Department of Materials Science and Engineering, University of Florida, Gainesville, Florida 32611, United States.

* Present address of corresponding author: Garstang 7.53, School of Biomedical Sciences, University of Leeds, Leeds LS2 9JT, United Kingdom.

E-mail address: k.k.narayanasamy@leeds.ac.uk.

Telephone number: +44 7454670404

Alternating current (AC) susceptibility as a particle-focused probe of coating and clustering behaviour in magnetic nanoparticle suspensions

Kaarjel K. Narayanasamy^{1,2,*}, Melissa Cruz-Acuña², Carlos Rinaldi², James Everett¹, Jon Dobson^{2,3}, Neil D. Telling¹

¹ Institute for Science and Technology in Medicine, Keele University, Stoke-on-Trent, Staffordshire ST4 7QB, United Kingdom.

² J. Crayton Pruitt Family Department of Biomedical Engineering, University of Florida, Gainesville, Florida 32611, United States.

³ Department of Materials Science and Engineering, University of Florida, Gainesville, Florida 32611, United States.

* Present address of corresponding author: School of Biomedical Sciences, University of Leeds, Leeds LS2 9JT, United Kingdom.

E-mail address: k.k.narayanasamy@leeds.ac.uk.

Telephone number: +44 7454670404

Abstract

Hypothesis

The functionality of magnetic nanoparticles (MNPs) relies heavily on their surface coating, which in turn affects the interactions between MNPs, and the formation of single-core particles or multi-core clusters. In this study we assessed the use of AC susceptibility (ACS) as a magnetic probe of the kinetics of coating and agglomeration of functionalised nanoparticles. We demonstrate the precision and sensitivity of ACS measurements to small changes in MNP coating using arginine-glycine-aspartic acid (RGD) tripeptide binding, and subsequently discuss how ACS can be used to optimise the preparation of polyethyleneimine (PEI) functionalised MNPs aimed at nanomagnetic transfection applications.

Experiments

We varied the PEI loading of suspensions of MNPs exhibiting a combination of Brownian and Néel relaxation, and used dialysis to study the movement of excess PEI during the coating process. Numerical ACS simulations were employed to determine particle cluster sizes and polydispersity and the results compared with conventional dynamic light scattering (DLS) size measurements.

Findings

ACS provided information on the MNP coating and agglomeration process that was not accessible through DLS due to the additional presence of non-magnetic polymer particulates in the suspensions. We consequently derived a simple method to obtain dense, uniform PEI coatings affording high-stability suspensions without excessive quantities of unbound PEI.

Keywords

AC susceptibility; magnetic nanoparticles; Brownian relaxation; hydrodynamic size; surface coating; particle clustering; polyethyleneimine (PEI); dynamic light scattering.

ACCEPTED MANUSCRIPT

Abbreviations:

MNPs, magnetic nanoparticles; PEI, polyethyleneimine; DLS, dynamic light scattering; ACS, AC susceptibility; RGD, arginine-glycine-aspartic acid; TEM, transmission electron microscopy; SEM, scanning electron microscopy; SEC, size exclusion chromatography; NTA, nanoparticle tracking analysis; EDAC, 1-Ethyl-3-(3-dimethylaminopropyl) carbodiimide chemistry (EDAC); NHS, N-Hydroxysuccinimide; MWCO, molecular weight cut-off; TGA, thermogravimetric analysis

1. Introduction

Magnetic nanoparticles (MNPs) are attractive for applications in biomedicine and bioengineering due to the ability to remotely direct their movement towards a target for cargo delivery, to harvest molecules, to act as contrast agent for diagnostics, or to induce localized heating such as hyperthermia^{1,2}. However, MNPs tend to agglomerate in suspension to minimise their surface energy. This property is not favourable in functional cellular studies as it can affect intrinsic magnetic properties as well as particle mobility in response to an applied magnetic field. Therefore, the surface of MNPs is usually modified to improve colloidal stability and to form homogeneous, bio-compatible aqueous suspensions. To avoid agglomeration, the MNP coating should prevent particle interactions such as magnetic forces between particles, and Van der Waals forces³. To promote colloidal stability, particles can be surface-modified with surfactants⁴, natural and synthetic polymers⁵, or biomolecules^{6,7}. In addition surface functionalization is used to facilitate binding and internalization of MNPs into cells for cell receptor targeting, or for gene or drug delivery for therapeutic purposes^{8,9}.

For nanomagnetic transfection applications, polyethyleneimine (PEI) is often used to coat the surface of MNPs in order to optimise their functionality^{10,11}. The presence of unbound PEI in MNP suspensions used for these applications is problematic as the excess PEI causes non-specific binding with DNA rather than DNA binding to the intended MNP surface, thus reducing the efficiency of nanomagnetic transfection¹². This can have a dramatic effect on the efficacy of the application as the MNP is required for improved transfection efficiency using magnetic targeting and sedimentation onto cell monolayers. PEI also causes cell toxicity, therefore removing excess PEI improves cell health^{13,14}.

Particle characterization is important in order to obtain physical and chemical information to understand the behaviour of MNPs in different systems and optimise performance for biomedical applications. In particular, particle size characterization is crucial for understanding particle-particle interaction, behaviour of particles embedded/suspended in different matrices, and changes in size distribution and agglomeration with different types of coatings. Common size characterization methods include dynamic light scattering (DLS), transmission electron microscopy (TEM), scanning electron microscopy (SEM), size exclusion chromatography (SEC), and nanoparticle tracking analysis (NTA)^{15,16}. DLS and NTA are the most frequently used methods to obtain the hydrodynamic diameter, D_H , which is a measure of the effective diffusive size of particles in liquid suspension. However, these methods measure all particulate material in the suspension, including material not associated with the MNPs of interest, such as coating fragments and buffer precipitates. When measuring magnetic nanoparticles, however, it is possible to use methods that are sensitive to the magnetic signal in order to isolate size information from the particles only.

Analogous to AC electronics, the AC magnetic susceptibility (ACS) signal is measured as a phasor with the form

$$\tilde{\chi} = \chi' + i\chi'' \quad (1)$$

where the real part, χ' , represents the susceptibility component of the particles that is in-phase with the applied AC magnetic field, and the imaginary part, χ'' , is the corresponding out-of-phase component. The relative proportion of the two components thus reveals the phase lag between the magnetisation of the particles and the applied AC field, with the case where χ' and χ'' are equal indicating a 45-degree phase angle.

ACS measurements are particularly important for observing magnetisation relaxation in magnetic nanoparticle suspensions. This is the process in which the initial magnetic alignment of the particles induced by the applied field is lost over a corresponding *relaxation time*, τ . For particles that are magnetically blocked (i.e. remain magnetised during an AC field cycle) relaxation is caused by the physical re-orientation of the particles due to collisions with molecules in the suspension media (i.e., Brownian motion). If we approximate the particles as spheres, then the corresponding Brownian relaxation time is given by

$$\tau_B = \frac{\pi\eta D_H^3}{2k_B T} \quad (2)$$

where η is the dynamic viscosity of the fluid, k_B is the Boltzmann constant and T is the absolute temperature. Thus, if all other parameters remain fixed, enlarging the hydrodynamic size (D_H) of the particles will increase the Brownian relaxation time.

Both the magnitude and the phase angle of the AC susceptibility depend on the product ($\omega\tau$) of the angular frequency of the AC field, ω , and the relaxation time, τ ¹⁷. However, whilst the phase angle gets larger as the frequency of the magnetic field increases, the corresponding magnitude of the susceptibility decreases. In fact, it can be shown that a maximum value of the out-of-phase component (χ'') is reached when $\omega\tau = 1$. For blocked particles, this condition will be reached when the Brownian relaxation time is equal to the rotational cycle time of the applied field. This is revealed as a peak in the χ'' susceptibility component when the frequency is swept. For larger hydrodynamic sizes, the correspondingly longer Brownian relaxation time will shift this peak to lower field frequency, as shown schematically in Figure 1. Thus, ACS measurements as a function of field frequency enable determination of the Brownian relaxation time and subsequently the hydrodynamic size of the particles using equation (2) above. Using this versatile characterization method, the formation of protein corona around MNPs caused by their surface charge^{18,19}, the aggregation of MNPs within polymer nanocomposites²⁰, and the mobility of MNPs in cells^{19,21,22}, have been explored previously.

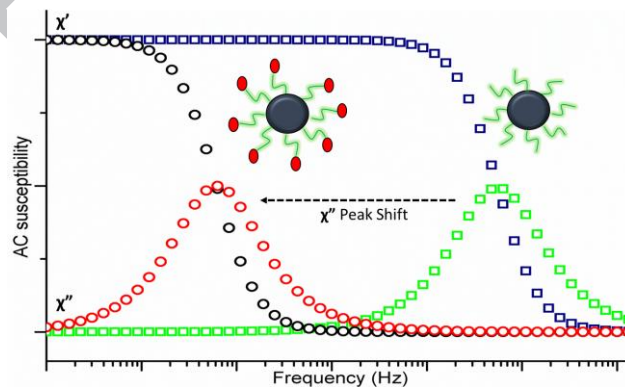


Figure 1: Schematic showing the AC susceptibility versus frequency curve expected for blocked magnetic nanoparticles displaying Brownian relaxation. Particles with small hydrodynamic sizes show a peak in the χ'' curve at high frequencies ($\chi'' =$ green, $\chi' =$ blue), whilst an increase in hydrodynamic size creates a shift of this peak to lower frequencies ($\chi'' =$ red, $\chi' =$ black).

Although the above discussion suggests a simple method for determining hydrodynamic sizes when blocked particles are present, more generally the suspensions will contain a distribution of particle sizes with both Brownian and Néel relaxation mechanisms possible. The latter effect is caused by the relaxation of the direction of the internal single magnetic domain of the particle and depends on the magnetic particle volume, the magnetic anisotropy property and the temperature of the system. However, it does not depend on hydrodynamic properties and so is insensitive to local environmental factors such as viscosity. The Néel relaxation time (τ_N) is given by the equation

$$\tau_N = \tau_0 e^{\left[\frac{KV}{k_B T}\right]} \quad (3)$$

where K is the magnetic anisotropy, V is the volume, k_B is the Boltzmann constant and T is the absolute temperature.

Maldonado-Camargo et al. derived simple equations to estimate the fractions of the two particle types, on the condition that both Brownian and Néel relaxation times were well separated²³. However, often the synthesis of MNP suspensions leads to a combination of magnetic and hydrodynamic particle sizes that results in relaxation by both mechanisms with an overlap in the corresponding χ'' peak positions. A method to characterize the mixture of MNP types in a suspension was developed by Ludwig et al. by applying a static magnetic field during an ACS measurement which was used to determine hydrodynamic and cores MNP sizes²⁴.

In this study, measurements of AC magnetic susceptibility were exploited as a particle-specific probe, demonstrating the sensitivity to small changes in the hydrodynamic size of commercial MNPs (showing largely Brownian relaxation behaviour) due to the addition of a thin layer of RGD tripeptide. Expanding on previous characterization studies of mixed MNP suspensions^{23,24}, we then monitored the progression of PEI coating and agglomeration of synthesized MNPs exhibiting both Brownian and Néel relaxation properties, where optimisation of these parameters is important for nanomagnetic transfection applications. ACS results were compared to simulations using a computational model of polydisperse nanoparticle clusters in order to determine the size distribution of both particles and clusters, and how these responded to different coating treatments. These results were compared to equivalent measurements using dynamic light scattering. Complementary characterisation using structural (TEM) and compositional (TGA) analysis techniques were used to confirm the interpretation from the ACS measurements and to provide additional parameters for the model. Furthermore, by monitoring the gradual coating of MNP suspensions using ACS measurements, an optimal ratio of coating material to MNPs can be determined in order to prepare uniformly-coated particles with minimal agglomeration, as well as reduce excess unbound coating material in the suspension.

2. Materials and Methods

2.1 RGD tripeptide coating of commercial MNPs

Dextran coated carboxyl-functionalised iron oxide MNPs (10 mg/mL) dispersed in water were purchased from micromod (Product code: 09-02-132). Materials were purchased from Sigma-Aldrich

and were used without further purification. Arginine-glycine-aspartic acid (RGD) tripeptide (97%) conjugation to MNPs was achieved via carbodiimide chemistry, through the addition of 1-Ethyl-3-(3-dimethylaminopropyl) carbodiimide chemistry (EDAC) and N-Hydroxysuccinimide (NHS)²⁵. 40 μ L of 6 mg/mL EDAC and 12 mg/mL NHS in 0.5 M 2-(*N*-morpholino) ethanesulfonic acid (MES) buffer (pH 6.3) was added to 200 μ L of carboxyl-functionalised MNPs, and was allowed to react for 1 hour at room temperature with gentle mixing. Particles were then magnetically separated, and the EDAC/NHS solution was removed. MNPs were resuspended in 0.1 M MES solution (pH 6.3) containing 250 μ g/mL RGD tripeptide and were incubated at 3°C overnight with continuous mixing. Following peptide conjugation particles were magnetically separated, and unreacted RGD solution was removed. RGD conjugated MNPs were resuspended in distilled water and stored at 3°C.

2.2 Synthesis of magnetic nanoparticles and dispersion in aqueous suspension

Reagents were purchased from Fisher Scientific unless stated otherwise. Purity of the reagents used were of at least analytical grade. Iron oxide magnetic nanoparticles were synthesized by the thermal decomposition method according to Cruz-Acuna et. al¹¹. Briefly, formation of the iron-oleate complex was performed by dissolving ferric (III) chloride hexahydrate (98%, Sigma-Aldrich) in deionized water with sodium oleate (99%, Sigma-Aldrich), hexane, and ethanol and heated at 67°C for 4 hours. The organic iron-oleate complex is evaporated to remove the aqueous phase and aged for 3 days at 60°C. Thermal decomposition of the iron-oleate complex is performed with oleic acid (99%, Sigma-Aldrich) and trioctylamine (98%, Sigma-Aldrich) at 335°C for 1 hour. The resulting magnetic nanoparticles were magnetically separated and suspended in toluene. Carboxylic acid functional groups were introduced to the oleic acid tails of the magnetic nanoparticles by oxidation with 0.28 M sodium periodate (99.8+%) in acetonitrile and ethyl acetate for 20 minutes under ultrasonication. Particles that underwent successful oxidation were magnetically separated and washed with ethanol. The MNPs were dried and resuspended in deionized water with ultrasonication for 2 hours to disperse particle clusters. The resulting particles formed stable aqueous suspensions.

2.3 PEI coating and dialysis of magnetic nanoparticles

PEI polymer of 25 kDa branched at pH 7 (Sigma-Aldrich; 408727) was used without further purification. Separate vials of 200 μ L of the aqueous MNP suspensions at a concentration of 0.3 mg/mL Fe prepared by thermal decomposition were coated with different mass of PEI polymer. To prepare the MNP-PEI coated suspensions, PEI (1 mg/mL) was added at volumes of 50, 500, 1000, and 2000 μ L to the 200 μ L MNP suspensions. These samples are hereafter referred to as *PEI 50*, *PEI 500*, *PEI 1000* and *PEI 2000* respectively. An uncoated suspension was also retained, referred to as *PEI 0*. All suspensions were sonicated with an ultrasonicator tip for 5 minutes prior to characterisation measurements. For dialysis experiments, suspensions were subsequently pipetted into separate dialysis tubes of 50 kDa molecular weight cut-off (MWCO; Sigma-Aldrich; PURX50005) which were placed in a 2 L container filled with distilled water and magnetically stirred overnight. The MNP suspensions were then concentrated using centrifugal concentrators of 30 kDa MWCO (Sigma-Aldrich; Z648035) prior to post-dialysis characterisation.

2.4 Dynamic light scattering

DLS measurements were performed using a Malvern zetasizer model 3000 HSA. MNP samples were diluted 5x to a final volume of 2 mL using distilled water and pipetted into a glass cuvette for DLS measurements. Intensity-weighted size distributions were converted to number-weighted distributions for analysis. MNP suspensions were measured before and after dialysis.

2.5 AC susceptibility measurements and simulations

AC susceptibility measurements were performed at 37°C on MNP suspensions both before and after dialysis, using an in-house built susceptometer capable of measuring at frequencies between 10 Hz and 1 MHz for highly concentrated ferrofluid samples (>1 mg/mL) (200 μ L volume). For more dilute samples the upper frequency limit is proportionally reduced due to the weak sample signal dropping below background. The volume susceptibility was obtained following background subtraction and calibration using a known mass of Dy₂O₃ powder.

Simulated AC susceptibility curves were obtained using a computational model that considers nanoparticle clusters in suspension, by summing the susceptibility calculated for each cluster. The model, which is described in detail elsewhere²⁶ creates clusters by selecting nanoparticles at random from a log-normal size distribution derived from input parameters for the particles. The generation of a log-normal size distribution of clusters is attempted by the model, based on input parameters for the clusters. However, the ability to form the intended cluster distribution depends on the match of the nanoparticle and cluster sizes and the computational limitations of the model. Thus, a log-normal fit to the actual cluster distribution created by the model (which was subsequently used to calculate the susceptibility) is reported here as the simulation parameter rather than the original input cluster parameters.

2.6 Transmission electron microscopy

TEM samples were prepared on copper mesh grids with carbon film (Agar Scientific; AGS160H). Synthesized MNP samples were diluted 50x in water from a concentration of 0.3 mg/mL Fe, and 5 μ L of the suspension was dropped onto the grid. The grid was dried by touching filter paper to the tip of the grid to absorb water and allowing it to air dry for 5 minutes. Samples were imaged on a JEOL100CXII for low resolution and Tecnai F30 for high resolution images. Particle distribution size analysis was performed using the Image J image processing software.

2.7 Thermogravimetric analysis

Thermogravimetric analysis (TGA) was performed with a TA instrument SDTQ600. Samples were pipetted into a 70 μ L alumina pan and dried in the oven at 70°C and subsequently cooled before measuring on the TGA. Dried samples were heated at a rate of increase of 5°C per minute under N₂ flow. The decrease in weight relative to temperature was analysed as organic PEI and moisture (Figure 2S in *supplemental information*).

2.8 Viscosity measurements

Viscosity measurements were performed at 37°C (to ensure consistency with ACS measurements) using a TA instrument AR-G2 Rheometer of 60 mm parallel plate geometry. Three PEI concentrations were prepared: 5 mg, 10 mg, and 20 mg PEI diluted in 22 mL distilled water, corresponding to PEI concentrations in sample *PEI 500*, *PEI 1000* and *PEI 2000 before dialysis*. Water, glycerol, and PEI at 1 mg/mL concentration were also measured as reference samples. The viscosity was determined from measurements in a shear rate range of 100 to 1000 1/s, for which all samples displayed constant viscosity. The viscosity values were included in ACS simulations for each sample (Table 1S in *supplemental information*).

3. Results and Discussion

The sensitivity of ACS to changes in the hydrodynamic size of MNPs in suspension is clearly demonstrated in Figure 2. In this case, commercial aqueous suspensions of magnetite MNP clusters with hydrodynamic diameters of 116 nm were measured before and after coating with the RGD tripeptide. As a result of the coating thickness, a small but clearly discernible shift in the frequency position of both the χ' and χ'' components can be seen in the figure. From equation (2) it can be shown that this shift corresponds to an increase in hydrodynamic diameter of only 6 nm, which is consistent with the expected coating thickness for this peptide. Owing to the reproducibility of the ACS measurements (Figure 1S in *supplemental information*), it should thus be possible to measure coating thicknesses of $< \sim 1$ nm for suitably sized particles.

For the large, 116 nm MNP clusters measured in Figure 2, the Brownian and Néel relaxation components are well separated, allowing a simple interpretation of the ACS data using equation (2). However, many MNP clusters required for biomedical applications, such as the PEI coated MNPs discussed below, have much smaller hydrodynamic sizes, due to the formation of small multi-core clusters or directly functionalised single-core MNPs. This can lead to a substantial overlap of the Brownian and Néel components making direct determination of hydrodynamic sizes more complicated. In the subsequent measurements, this effect was observed using lab-synthesized MNPs and the size-distribution was determined using ACS simulations.

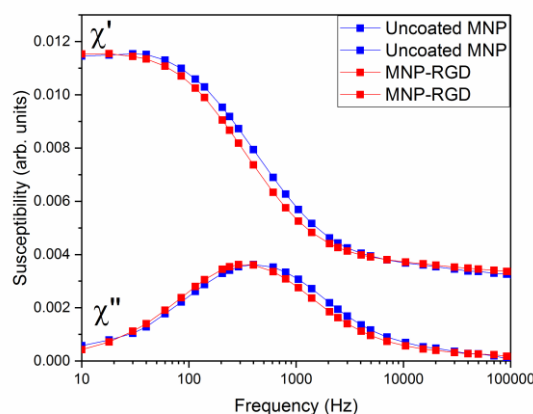


Figure 2: AC susceptibility from an aqueous suspension of magnetite MNPs measured before and after coating with RGD tripeptide.

PEI coating studies were performed using MNPs synthesised using a thermal decomposition method¹¹. TEM images were obtained for synthesised iron oxide MNPs (Figure 3a), showing them to be mainly spherical and relatively monodisperse, with a small proportion of smaller irregular shaped particles. Particle size distributions were obtained from TEM images by measuring the diameter of ~1000 particles using image processing software, and the histogram fitted with a lognormal distribution (Figure 3b). The average particle core diameter was found to be 17.4 nm with 15% polydispersity.

PEI can attach weakly onto the surface of carboxylic acid functionalised MNPs due to ionic interactions between the negative charges of the COO^- functional groups with the positively charged NH_3^+ groups of PEI. Figure 4 demonstrates the effect of sonication during MNP surface coating with PEI, measured before and after sonication with the addition of 500 μg of PEI to a 200 μL suspension of 1.3 mg/mL Fe of MNPs. There is an obvious χ'' peak shift in all 3 samples, starting with sample *PEI 0* (Figure 4, top) with a peak position at the far right (~45 kHz) followed by a large shift to 66 Hz with the addition of PEI (Figure 4, middle), and peak movement back to >10 kHz after sonication (Figure 4, bottom). The χ'' curve of the MNP-PEI sample before sonication (Figure 4, middle) intercepts the y-axis above zero, indicating that a portion of the particle sample is highly clustered with a Brownian relaxation frequency below the measurement limit of 10 Hz. After sonication, the χ'' peak shows a strong shift back towards higher frequencies.

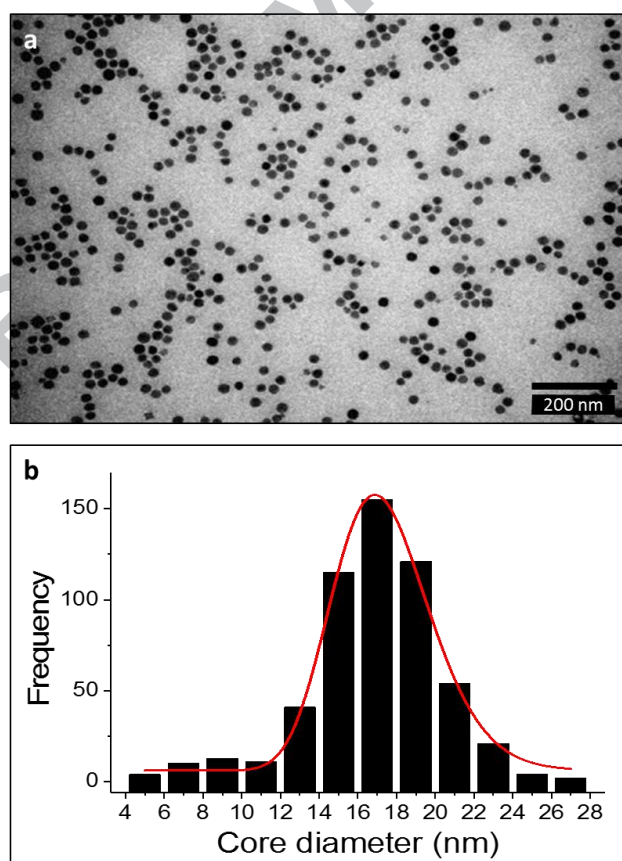


Figure 3: (a) TEM micrograph showing MNP core size distribution and shape and (b) histogram of MNP core diameter distribution fitted with a lognormal curve.

From Figure 4 it can be seen that each MNP treatment resulted in a Brownian frequency peak shift, indicating changes in the hydrodynamic size of the agglomerates. The sample without PEI coating (referred to as *PEI 0*) was a stable colloid in water with negatively charged oleic acid surface coating which provided ionic and some steric hindrance stability (Figure 4, top). The addition of positively charged PEI into the MNP suspension resulted in the formation of particulates with large hydrodynamic sizes, based on the low frequency χ'' peak position (Fig 4, middle). The large size could indicate particle agglomeration and clustering due to uneven PEI coating around multi-core particles (Figure 4, middle). Another possibility is the assembly of multiple PEI layers forming a thick coating around individual MNPs.

Strong sonication of the MNP-PEI suspension appeared to induce MNP dispersion/de-clustering resulting in smaller particulates as revealed by the reduced hydrodynamic size (Figure 4, bottom). It is also possible that the PEI surrounding the particles could be redistributed at this stage. This hypothetical mechanism for the PEI coating process is illustrated schematically on the right-hand side of Figure 4.

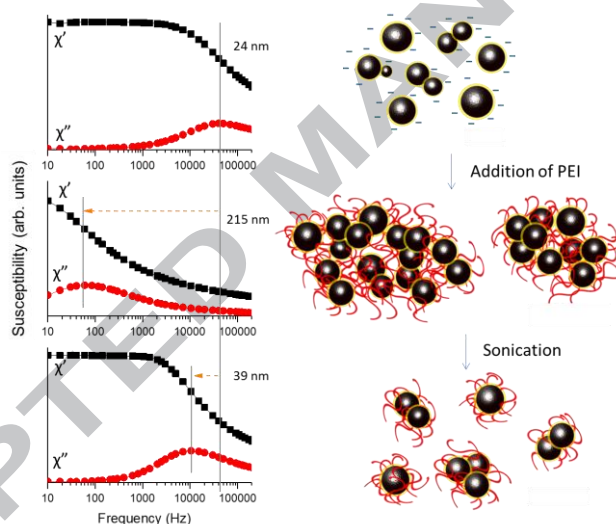


Figure 4: AC susceptibility measurements from: MNPs before PEI coating, sample *PEI 0* (top), after PEI addition (middle), and after PEI addition and sonication (bottom). For each treatment, the hydrodynamic size of the particle or agglomerate was estimated from the frequency position of the χ'' peak using the Brownian relaxation time equation (2) above.

To investigate these effects further, the changes in particle size and clustering with gradual loading of surface coating were considered. Four different PEI to MNP mass ratios were prepared where 50, 500, 1000, and 2000 μL of 1 mg/mL PEI were added into 200 μL MNP suspensions of 0.3 mg/mL Fe (*PEI 0*) and sonicated to disperse agglomerates. These samples are referred to as *PEI 50*, *PEI 500*, *PEI 1000*, and *PEI 2000*. As the Brownian relaxation depends on suspension viscosity (see equation 2 above), it was necessary to measure the viscosity of PEI in water at concentrations corresponding to that present in the MNP samples (detailed in Materials and Methods). This was done using rheology and the values obtained were used later in the AC susceptibility simulations (Table 1S in supplemental information).

TEM was also performed on the samples. Figures 5a and 5b show the distribution of uncoated MNP cores (*PEI 0*) which are spherical and have a relatively narrow size distribution compared to MNPs synthesized by the well-known co-precipitation method. The particles are also mainly singly distributed or paired with no significant agglomeration, due to their stable oleic acid coating. In Figure 5b, the high resolution TEM does not show coating around the MNPs, as the oleic acid coating is too thin to observe, or the low electron density of oleic acid provided little contrast compared to the MNPs.

Figures 5c and 5d show sample *PEI 50*. Close observation reveals uneven layers of PEI polymer binding to the particles (indicated by red arrows), resulting in the formation of large agglomerates. This overall PEI coating may surround the agglomerate leading to the measurement of positive zeta potential discussed earlier. In contrast a more uniform PEI coating can be seen in sample *PEI 1000* (Figure 5e and 5f). Here the PEI coating surrounding each particle can be seen clearly, with space between the particles due to steric hindrance of the polymer. The added polymer coating affords a higher level of stability to the particles in water compared to oleic acid coated particles, due to stronger steric hindrance and electrostatic repulsion between particles, resulting in reduced agglomeration.

Although the TEM results support the hypothetical mechanism for PEI coating of the MNPs shown in Figure 4, the interpretation of such micrographs must be approached with caution as agglomeration can also occur when the samples dry during TEM specimen preparation, especially at the edges (Figure 5c). To measure the MNP coating and agglomeration effects *in suspension*, we compared the effectiveness of AC susceptibility measurements and DLS on all samples.

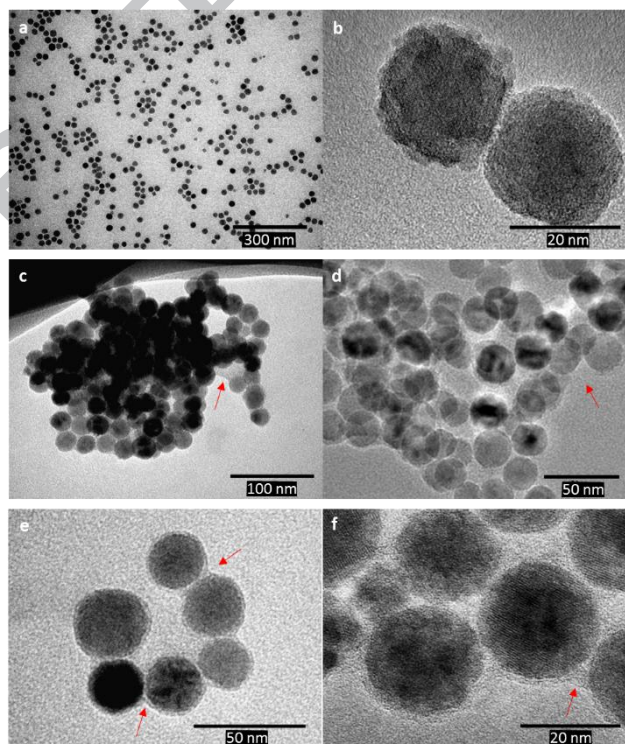


Figure 5: TEM micrographs of MNP samples of (a) and (b) *PEI 0* without PEI coating, (c) and (d) *PEI 50* showing MNP agglomeration, and (e) and (f) *PEI 1000* with even PEI coating around MNP. Red arrows indicate a layer of PEI coating around MNPs.

In addition to the effect of PEI loading, samples of uncoated MNPs, partially agglomerated MNPs, and well-coated MNPs were prepared using the dialysis method, which were then modelled using ACS measurements. Dialysis was also used to understand the presence of free or loosely bound PEI in the suspensions with high PEI loading and movement of PEI between MNP samples. During dialysis, passive diffusion occurs due to a concentration gradient, which generates movement of unbound PEI from high PEI concentration in the dialysis tube to low concentration in the dialysate (distilled water). This allows unbound PEI to be removed from the MNP-PEI suspension, leaving only PEI attached to the particles.

Dialysis is relatively gentle and so is less likely to strip PEI attached to particles, nor subject the samples to harsh treatments such as strong forces with repetitive centrifugal filtration which may clump particles at the bottom of the filter, or magnetic separation columns which can strip weakly bound/physisorbed coating off due to strong shear flow of washing solutions, and which also requires a large amount of sample. Dialysis was used to model the movement PEI polymers between PEI coated MNP samples and the uncoated control MNPs.

For this experiment, dialysis tubes containing samples of all PEI loadings (including the uncoated *PEI 0* sample) were placed in a shared dialysate to study the binding and redistribution of PEI between samples.

To confirm the presence of bound PEI on the MNP surfaces after the dialysis process, TGA measurements were performed (Figure 6). Here the sample is heated continuously and the change in mass is monitored as a function of temperature. Oleic acid shows complete degradation at 200°C (*supplementary information*), however sample *PEI 0* (Figure 6) which only has oleic acid coating does not show a noticeable decrease in weight after heating, which could be attributed to the small amount of oleic acid relative to weight of the MNP core.

Figure 6 shows a majority 3-step decay of PEI coated MNP samples. The first weight loss step plateaus at around 200°C which corresponds to evaporation of sample moisture²⁷. Since oleic acid also undergoes thermal degradation at the same temperature, the weight difference between moisture and oleic acid is indistinguishable. The second step decay is from 200°C to 400°C and contributes to the highest percentage of weight loss for samples *PEI 1000* and above. This step is due to the decomposition of PEI and appears to scale with the designed PEI loading, with *PEI 2000* showing the largest step whilst *PEI 50* shows only a modest effect. This shows that even after dialysis, *PEI 1000* and *PEI 2000* samples still had the highest PEI loading and the PEI coating on MNPs were retained after dialysis.

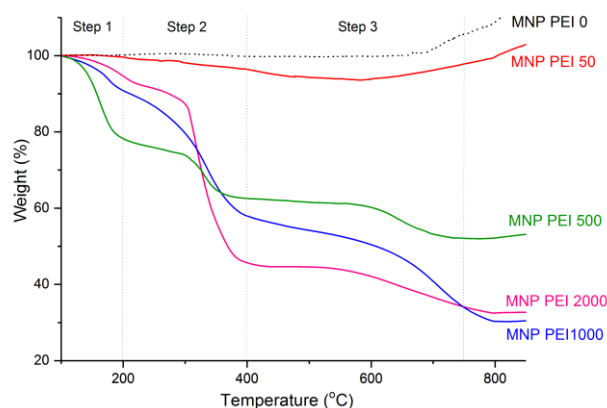


Figure 6: TGA analysis of samples PEI 0 (black dotted line) without PEI loading as a control sample, and samples PEI 50, PEI 500, PEI 1000, and PEI 2000 after dialysis (solid lines).

The measured zeta potential of the samples before and after dialysis is shown in Table 1. The zeta potential of sample PEI 0 before dialysis was -38 mV, due to the contribution of the COOH functional groups. PEI 0 after dialysis had a zeta potential close to zero, indicating that loosely or unbound PEI in the dialysate had permeated into the sample suspension and bound to the negatively charged PEI 0 MNPs. The positively charged amine group on the PEI thus neutralized the carboxylic charge, giving a net zeta potential of ~ 0 mV. For the PEI coated MNPs (PEI 50, 500, 1000, and 2000) before dialysis, the surface charge was large and positive at around $+30$ to $+40$ mV indicating a degree of surface coverage of the PEI around the MNPs. After dialysis these values became more positive at around $+50$ to $+60$ mV, suggesting a denser packing of the PEI on the MNP surface probably due to the redistribution of loosely bound PEI. Increased condensation of PEI polyplexes have been shown to contribute to higher charge density²⁸.

Table 1: Zeta potential measurements of the surface charge of MNP-PEI samples after sonication, before and after dialysis.

	Zeta Potential (mV) (± 4)				
	PEI 0	PEI 50	PEI 500	PEI 1000	PEI 2000
Before dialysis	-38	+34	+36	+30	+40
After dialysis	-4	+56	+48	+59	+53

As discussed earlier, polydisperse MNP suspensions can lead to a combination of Brownian and Néel relaxation mechanisms, complicating interpretation of the ACS curves. In order to analyse the changes occurring in the suspensions at each treatment stage, simulations were performed using the modelling parameters shown in Table 1S (supplemental information). Parameters relating to the

individual magnetic particle properties (e.g. mean size, anisotropy) were fixed for all treatments and were determined based on initial fitting to the ACS data from the *PEI 0* sample, as well as from TEM measurements. The effects of combined Brownian and Néel relaxation mechanisms can be seen in Figure 7, where the best-fit simulation curve is compared to the data from *PEI 0* (middle plot). The effective magnetic anisotropy constant for the particles was determined to be 7200 Jm^{-3} , which is consistent with oxidised magnetite nanoparticles.

The equivalent results expected if the suspension contained either only blocked particles (Brownian relaxation), or predominately particles relaxing by the Néel mechanism, was simulated by increasing or decreasing the anisotropy constant respectively (see Table 1S in *supplemental information*). These simulations are compared to the data in Figure 7 (top and bottom plots respectively) and show how both the apparent position as well as the intensity of the χ'' peak is affected by the magnetic properties of the particles. The best-fit curve was obtained by modelling a log-normal distribution of nanoparticle clusters with a mean diameter of 20.4 nm. This value is only slightly larger than the mean nanoparticle diameter of 17.4 nm, which is consistent with the formation of small clusters in suspension containing one or occasionally two particles, as suggested by the TEM images earlier (Figures 5a and 5b).

This analysis was extended to the PEI sample series where the change in viscosity of the suspensions with significant addition of PEI (i.e., samples *PEI 500*, *PEI 1000* and *PEI 2000*) before dialysis, was explicitly included in the model (see Table 1S in *supplemental information*). From equation (2) it can be seen that if instead the viscosity is assumed to be that of water, the calculated hydrodynamic diameter of the clusters will be ~20% higher than that obtained using the viscosity values shown in Table 1S (*supplemental information*).

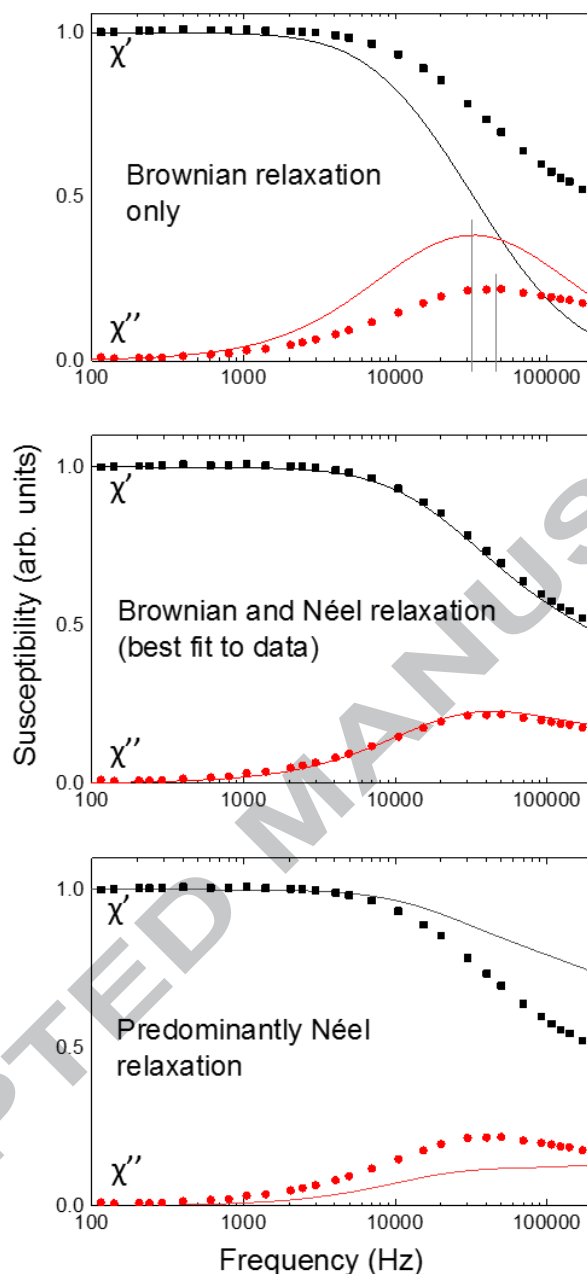


Figure 7: ACS measurements of sample PEI 0 before dialysis (symbols) compared to simulated data (solid lines) obtained by fitting the cluster size distribution and polydispersity. The middle plot shows the best-fit data whilst the magnetic anisotropy used in the simulations was varied to produce the expected result for particles undergoing purely Brownian relaxation (top) or predominantly Néel relaxation (bottom).

The ACS data measured before and after dialysis, together with best-fit simulation curves are shown for the PEI 0, PEI 50 and PEI 2000 samples in Figure 8a. In all cases a close fit was obtained. In particular, the simulations reproduce the changes to the peak positions and breadths for different treatments. The corresponding log-normal distributions of cluster sizes determined in each case are shown in Figure 8b, whilst the results obtained for the full sample set are given in Table 2.

From the results shown in Figure 8b and Table 2 it can be seen that the addition of small amounts of PEI (as is the case for sample *PEI 50*) leads to a substantial increase in the mean cluster size from 20.4 nm to 31.7 nm, as well as an increase in the polydispersity of the clusters from 0.30 to 0.44. This is consistent with an insufficient amount of PEI to uniformly coat particles individually. PEI therefore wraps around clusters of particles creating multi-core agglomerates and this results in instability and sample flocculation. This can be seen more dramatically for sample *PEI 0* after dialysis, where a similar increase in mean cluster size was determined but with a very large polydispersity index (0.60) suggesting a highly agglomerated and destabilised sample. As this sample contains no PEI, in this case the effect must be caused by free PEI diffusing along the concentration gradient from the dialysate, as suggested earlier by the neutralisation of the zeta potential. The *PEI 0* sample thus acted as an indicator of the dialysis process, confirming the movement of free and loosely bound PEI from the other samples, inducing agglomeration similar to sample *PEI 50*.

The *PEI 50* sample also shows an increase in the mean cluster diameter after dialysis, again suggesting an influx of free PEI from the dialysate. This is not unexpected as there should be little free PEI in this sample and thus the concentration gradient is present, similar to *PEI 0*. However, the higher loading PEI samples (*PEI 500* and above) show no real change in mean cluster diameter after dialysis, and only a modest increase in polydispersity. Of particular interest, the mean cluster diameter is very similar to that determined for the stable uncoated particles (*PEI 0*). The stabilization in cluster size at high PEI loading indicates coating saturation on the surface of MNPs, therefore additional loading of PEI will not lead to a further increase in MNP hydrodynamic size. Although it is possible that some free PEI remains in the suspensions after dialysis, in our analysis we approximated the viscosity as being the same as for water for these samples (Table 1S in *supplemental information*). If a viscosity larger than water was used to determine the cluster sizes after dialysis, a value smaller than that measured for the original stable uncoated particles (*PEI 0*) would be obtained. As this result seems extremely unlikely, the assumptions made regarding the viscosity after dialysis would appear to be valid.

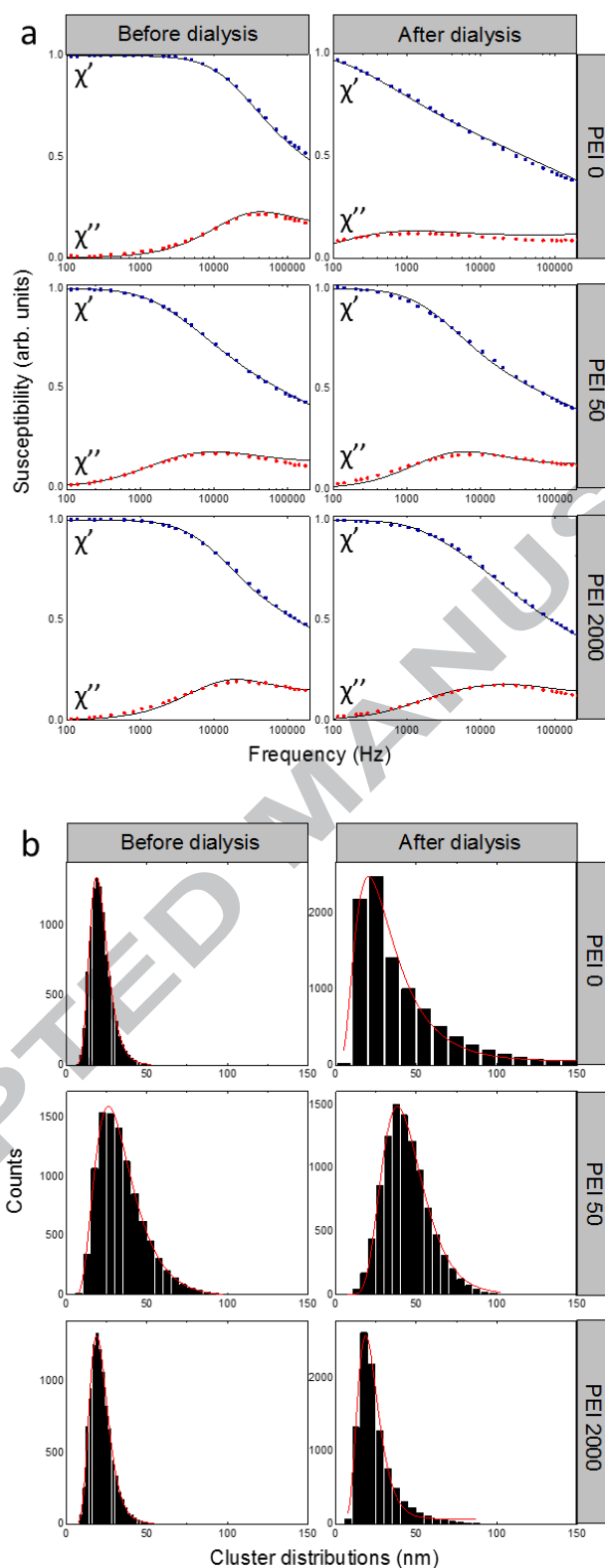


Figure 8: (a) ACS measurements from samples PEI 0, PEI 50, and PEI 2000 obtained both before and after dialysis (symbols), together with best-fit simulations. (b) Histograms showing the lognormal MNP cluster distributions used to obtain the best-fit ACS curves shown in Figure 7a.

Table 2: Mean cluster diameter and polydispersity index of determined from all MNP suspensions in as-prepared state and after dialysis, obtained from best-fit simulations to the measured AC susceptibility data. Errors shown represent the uncertainties estimated from the uniqueness of the simulation fits.

Sample		Mean cluster diameter (nm) \pm 0.2	Polydispersity Index \pm 0.01		Mean cluster diameter (nm) \pm 0.2	Polydispersity Index \pm 0.01
PEI 0	As prepared	20.4	0.30	After dialysis	29.1	0.60
PEI 50		31.7	0.44		42.7	0.33
PEI 500		22.2	0.32		21.8	0.36
PEI 1000		20.4	0.30		21.0	0.34
PEI 2000		20.6	0.30		20.9	0.35

The corresponding hydrodynamic sizes obtained by DLS are shown in Figure 9. It can be seen that the trend in the values measured before dialysis is nearly identical to that found with the ACS measurements, but with hydrodynamic sizes \sim 30% larger than the corresponding cluster diameters determined from ACS. However, evidence of some much larger particles can also be seen (for example *PEI 2000 before dialysis*). As particles of such size are not seen in the ACS measurements, it is possible that these represent the formation of pure PEI polyplexes that are not detected by ACS.

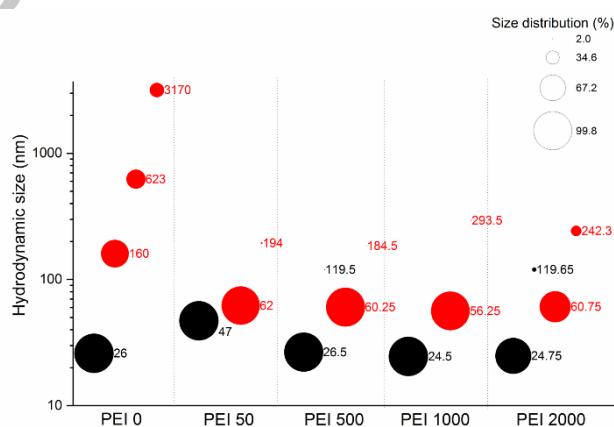


Figure 9: DLS hydrodynamic size measurements of MNP-PEI samples before dialysis (black) and after dialysis (red). The viscosity values are given in Table 1S (supplemental information).

The agreement with the ACS data is far worse for the samples measured after dialysis. In particular a large proportion of very large particles (>160 nm) was observed for sample *PEI 0 after dialysis*. As evidence was found for free PEI diffusion into this sample, it is likely that DLS includes measurement of the resulting polydisperse PEI-MNP agglomerates as well as a proportion of PEI polyplexes, thus making an assessment of MNP cluster sizes impossible. In a similar fashion the DLS measurement indicates much larger particle sizes than ACS for the PEI coated MNPs after dialysis. Thus, the different values determined by the two techniques could be due to the disproportionate response of DLS to large particles, which can tend to skew the calculated hydrodynamic size distributions.

4. Conclusion

This study demonstrates that AC susceptibility is a sensitive and precise method to measure changes in the coating and agglomeration of MNPs in complex suspensions, even when both Brownian and Néel relaxation mechanisms are present. In particular, as the technique is sensitive to only the magnetic signal in the suspension, it is possible to separate the behaviour of the MNPs from that of other particulates in the suspension. This enables insight into complex MNP suspensions where conventional techniques such as DLS are compromised by the presence of other species such as PEI polyplexes. The value of this approach is demonstrated here with regard to defining a new methodology for optimising the PEI coating of MNPs for gene transfection applications.

Conventional characterization techniques provide limited information regarding MNP-coating density and the presence of non-interacting/unbound material in a colloid^{10,29}. By combining AC susceptibility with other characterisation techniques such as zeta potential measurements, TEM, and TGA, on MNPs coated with increasing concentrations of PEI, it was possible to determine the optimum ratio of MNPs to PEI to obtain small MNP clusters with dense PEI coatings. This is important for nanomagnetic gene transfection applications, where good control over the plasmid binding to the PEI-coated MNPs is essential to optimise the effectiveness of the application. In particular, non-specific binding of plasmid to free PEI in the suspension must be avoided as this suppresses the effectiveness of the magnetic targeting and so lowers transfection efficiency, as well as causing additional cytotoxicity^{30,31}.

The results showed that the combination of PEI loading and sonication results in the formation of clusters of similar size to the original uncoated MNP clusters, with stable high-density coating resulting in high zeta potential values of ~+50 mV. This method effectively reduces the presence of free/unbound PEI in the suspension as well as eliminates the washing step during the coating process, which is not only cost effective but also reduces particle agglomeration and polyplex formation that occurs during harsh washing procedures.

Furthermore, evidence from ACS and zeta potential measurements also suggested that dialysis facilitated the movement of free/unbound PEI between samples without compromising the coating and stability of PEI attached to MNPs. Therefore, dialysis would be a suitable washing method during MNP coating procedures as an alternative to centrifugal filtration and magnetic separation. The resulting uniform and highly stable PEI coated MNPs are ideally suited to applications in nanomagnetic gene transfection applications.

Ultimately, ACS could be incorporated into standard research methodology for the characterisation of functionalised MNPs for biomedical applications, as well as forming a key step in quality control for scaled up industrial processes. Future developments of the instrumentation could see miniaturised AC susceptibility hardware incorporated into lab-on-a-chip and continuous flow systems, enabling a step change in the ability to prepare optimally functionalised MNPs to target specific biomedical applications.

Acknowledgements

The authors would like to acknowledge the Marie Curie Intra-European Fellowship within the 7th European Community Framework: Functionalized Magnetic Nanoparticles and Their Application on Chemistry and Biomedicine (MAGNETICFUN), Grant Number 290248. In addition, we extend our appreciation to Dr Lorena Maldonado of the University of Florida for assisting with MNP synthesis.

Declarations of interest: none

References

1. Pankhurst, Q. A., Connolly, J., Jones, S. K. & Dobson, J. Applications of magnetic nanoparticles in biomedicine. *J. Phys. D. Appl. Phys.* **36**, R167–R181 (2003).
2. Sensenig, R., Sapir, Y., MacDonald, C., Cohen, S. & Polyak, B. Magnetic nanoparticle-based approaches to locally target therapy and enhance tissue regeneration in vivo. *Nanomedicine* **7**, 1425–1442 (2012).
3. Mahmoudi, M., Sant, S., Wang, B., Laurent, S. & Sen, T. Superparamagnetic iron oxide nanoparticles (SPIONs): development, surface modification and applications in chemotherapy. *Adv. Drug Deliv. Rev.* **63**, 24–46 (2011).
4. Ramimoghadam, D., Bagheri, S. & Abd Hamid, S. B. Stable monodisperse nanomagnetic colloidal suspensions: An overview. *Colloids Surfaces B Biointerfaces* **133**, 388–411 (2014).
5. Shaterabadi, Z., Nabiyouni, G. & Soleymani, M. High impact of in situ dextran coating on biocompatibility, stability and magnetic properties of iron oxide nanoparticles. *Mater. Sci. Eng. C* **75**, 947–956 (2017).
6. Aires, A., Cabrera, D., Alonso-Pardo, L. C., Cortajarena, A. L. & Teran, F. J. Elucidation of the Physicochemical Properties Ruling the Colloidal Stability of Iron Oxide Nanoparticles under Physiological Conditions. *ChemNanoMat* **3**, 183–189 (2017).
7. Yu, S.-M., Laromaine, A. & Roig, A. Enhanced stability of superparamagnetic iron oxide nanoparticles in biological media using a pH adjusted-BSA adsorption protocol. *J. Nanoparticle Res.* **16**, 2484 (2014).
8. McBain, S. C., Yiu, H. H. P. & Dobson, J. Magnetic nanoparticles for gene and drug delivery. *Int. J. Nanomedicine* **3**, 169–180 (2008).
9. Kang, T. *et al.* Surface design of magnetic nanoparticles for stimuli-responsive cancer imaging and therapy. *Biomaterials* **136**, 98–114 (2017).

10. Zhang, L., Li, Y., Yu, J. C., Chen, Y. Y. & Chan, K. M. Assembly of polyethylenimine-functionalized iron oxide nanoparticles as agents for DNA transfection with magnetofection technique. *J. Mater. Chem. B* **2**, 7936–7944 (2014).
11. Cruz-Acuna, M., Maldonado-Camargo, L., Dobson, J. & Rinaldi, C. From oleic acid-capped iron oxide nanoparticles to polyethyleneimine-coated single-particle magnetofectins. *J. Nanoparticle Res.* **18**, 268 (2016).
12. Arsianti, M., Lim, M., Marquis, C. P. & Amal, R. Assembly of polyethylenimine-based magnetic iron oxide vectors: insights into gene delivery. *Langmuir* **26**, 7314–26 (2010).
13. Godbey, W. T., Wu, K. K. & Mikos, A. G. Poly(ethylenimine) and its role in gene delivery. *J. Control. Release* **60**, 149–160 (1999).
14. Godbey, W. T., Wu, K. K. & Mikos, A. G. Poly(ethylenimine)-mediated gene delivery affects endothelial cell function and viability. *Biomaterials* **22**, 471–480 (2001).
15. Lim, J., Yeap, S., Che, H. & Low, S. Characterization of magnetic nanoparticle by dynamic light scattering. *Nanoscale Res. Lett.* **8**, 381 (2013).
16. Trekker, J. *et al.* Synthesis of PEGylated magnetic nanoparticles with different core sizes. *IEEE Trans. Magn.* **49**, 219–226 (2013).
17. Carrey, J., Mehdaoui, B. & Respaud, M. Simple models for dynamic hysteresis loop calculations of magnetic single-domain nanoparticles: Application to magnetic hyperthermia optimization. *J. Appl. Phys* **109**, 83921 (2011).
18. Bohorquez, A. C. & Rinaldi, C. In Situ Evaluation of Nanoparticle – Protein Interactions by Dynamic Magnetic Susceptibility Measurements. *Part. Part. Syst. Charact.* **31**, 561–570 (2014).
19. Soukup, D., Moise, S., Céspedes, E., Dobson, J. & Telling, N. D. In situ measurement of magnetization relaxation of internalized nanoparticles in live cells. *ACS Nano* **9**, 231–40 (2015).
20. Sierra-bermúdez, S., Maldonado-camargo, L. P., Orange, F., Guinel, M. J. & Rinaldi, C. Assessing magnetic nanoparticle aggregation in polymer melts by dynamic magnetic susceptibility measurements. *J. Magn. Magn. Mater.* **378**, 64–72 (2015).
21. Moise, S. *et al.* The cellular magnetic response and biocompatibility of biogenic zinc- and cobalt-doped magnetite nanoparticles. *Nat. Publ. Gr.* **7**, 1–11 (2017).
22. Cabrera, D. *et al.* Influence of cell uptake on the dynamical magnetic response of iron oxide nanoparticles. *ACS Nano* **Accepted**, (2018).
23. Maldonado-Camargo, L., Torres-Díaz, I., Chiu-Lam, A., Hernández, M. & Rinaldi, C. Estimating the contribution of Brownian and Neel relaxation in a magnetic fluid through dynamic magnetic susceptibility measurements. *J. Magn. Magn. Mater.* **412**, 223–233 (2016).
24. Ludwig, F., Guillaume, A., Schilling, M., Frickel, N. & Schmidt, A. M. Determination of core and hydrodynamic size distributions of CoFe₂O₄ nanoparticle suspensions using ac susceptibility measurements. *J. Appl. Phys.* **108**, 33918 (2010).
25. Hermanson, G. T. *Bioconjugate Techniques, 3rd edition.* (Academic Press, 2013).
26. Céspedes, E. *et al.* Bacterially synthesized ferrite nanoparticles for magnetic hyperthermia applications. *Nanoscale* **6**, 12958–12970 (2014).

27. Kapilov-Buchman, Y., Lellouche, E., Michaeli, S. & Lellouche, J.-P. Unique Surface Modification of Silica Nanoparticles with Polyethylenimine (PEI) for siRNA Delivery Using Cerium Cation Coordination Chemistry. *Bioconjug. Chem.* **26**, 880–889 (2015).
28. Amin, Z. R., Rahimizadeh, M., Eshghi, H., Dehshahri, A. & Ramezani, M. The effect of cationic charge density change on transfection efficiency of Polyethylenimine. *Iran. J. Basic Med. Sci.* **16**, 150–156 (2013).
29. Sohrabijam, Z., Saeidifar, M. & Zamanian, A. Enhancement of magnetofection efficiency using chitosan coated superparamagnetic iron oxide nanoparticles and calf thymus DNA. *Colloids Surfaces B Biointerfaces* **152**, 169–175 (2017).
30. Lv, H., Zhang, S., Wang, B., Cui, S. & Yan, J. Toxicity of cationic lipids and cationic polymers in gene delivery. *J. Control. Release* **114**, 100–109 (2006).
31. Boeckle, S. *et al.* Purification of polyethylenimine polyplexes highlights the role of free polycations in gene transfer. *J. Gene Med.* **6**, 1102–1111 (2004).

Graphical Abstract

AC susceptibility as a particle-focused probe of coating and clustering behaviour in magnetic nanoparticle suspensions

Kaarjel K. Narayanasamy^{1,2,*}, Melissa Cruz-Acuña², Carlos Rinaldi², James Everett¹, Jon Dobson^{2,3}, Neil D. Telling¹

¹ Institute for Science and Technology in Medicine, Keele University, Stoke-on-Trent, Staffordshire ST4 7QB, United Kingdom.

² J. Crayton Pruitt Family Department of Biomedical Engineering, University of Florida, Gainesville, Florida 32611, United States.

³ Department of Materials Science and Engineering, University of Florida, Gainesville, Florida 32611, United States.

* Present address of corresponding author: School of Biomedical Sciences, University of Leeds, Leeds LS2 9JT, United Kingdom.

E-mail address: k.k.narayanasamy@leeds.ac.uk.

Telephone number: +44 7454670404

